ECMWF Feature article

from Newsletter Number 181 – Autumn 2024

EARTH SYSTEM SCIENCE

IFS upgrade improves near-surface wind and temperature forecasts

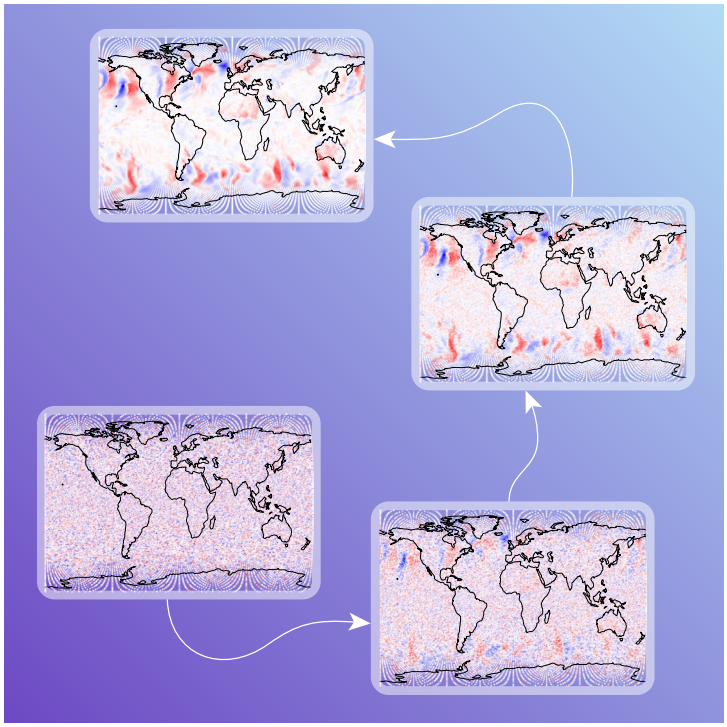

www.ecmwf.int/en/about/media-centre/media-resources

doi: 10.21957/crx2bn4is8

This article appeared in the Earth system science section of ECMWF Newsletter No. 181 – Autumn 2024, pp. 16–25

IFS upgrade improves near-surface wind and temperature forecasts

Christopher D. Roberts, Bruce Ingleby, Alan Geer, Elias Hólm, Martin Janousek, Fernando Prates, Mark Rodwell

The latest update to the ECMWF Integrated Forecasting System (IFS) is due to be implemented operationally in November 2024.IFS Cycle 49r1 is a major upgrade to the IFS model and associated data assimilation system. Among many other changes, it includes the assimilation of 2 m temperature observations; increased resolution and soft re-centring of the Ensemble of Data Assimilations (EDA); activation of the Stochastically Perturbed Parametrizations (SPP) scheme for model uncertainty in all ensemble applications; extended use of microwave data over sea ice; higher-resolution data from infrared satellite sounders; and improvements to land-surface modelling and assimilation methodology. This upgrade substantially improves 2 m temperature and 10 m wind speeds, particularly for the winter months in the northern hemisphere. Cycle 49r1 also brings changes to the resolution of the ocean wave model and the frequency of medium-range and sub-seasonal re-forecasts, which will now run on fixed days of the month.

Forecast model

An essential ingredient of a reliable ensemble forecast system is an accurate representation of the uncertainties associated with parametrized physical processes. One of the major changes in IFS Cycle 49r1 is the activation of the Stochastically Perturbed Parametrizations (SPP) scheme, which replaces the effective and long-serving Stochastically Perturbed Parametrization Tendencies (SPPT) scheme in all ensemble configurations. The main impacts of the switch to SPP include:

- improved physical consistency due to local conservation of moisture and energy, which was not respected by SPPT
- an improved representation of uncertainties in the near-surface boundary layer, which contributes to improved probabilistic skill of 2 m temperature and 10 m winds in medium-range forecasts
- improvements to the spread–error relationship of sub-seasonal forecasts of the Madden–Julian Oscillation (MJO), and
- an increase in the frequency of tropical cyclones (TCs).

Further information about this revision of the IFS model uncertainty scheme, including the scientific motivations and implementation details, are provided by Leutbecher et al. in this Newsletter.

Cycle 49r1 includes several scientific and technical changes to the ocean wave model, including a revision of the horizontal grid to match the atmosphere resolution in all forecasts. This corresponds to a reduction of the wave model grid spacing to ~9 km (TCo1279) in medium-range forecasts and ~36 km (TCo319) in sub-seasonal forecasts. To make this increased resolution affordable, the number of frequencies in wave spectra output (but not online computations) is reduced from 36 to 29 frequencies. The most significant scientific changes are to the wind input parametrizations, including a new gravity–capillary model and non-linear growth rates. These updates modulate variations in the drag coefficient with wind speed, which addresses a known underestimation of extreme ocean wind speeds. There are also new sea-state-dependent heat and moisture fluxes. These changes have a strong impact on air temperatures over the oceans throughout the troposphere, primarily in the tropics and winter hemisphere (Bidlot & Janssen, 2024).

The land surface benefits from several IFS model updates introduced in Cycle 49r1. These include a single-layer urban canopy model implemented as a new surface tile, which improves 2 m temperature and 10 m wind speed forecasts over urban areas (McNorton & Balsamo, 2023). Vegetation and leaf-area index maps are updated with new versions from the European Space Agency (ESA) Climate Change Initiative and the new Copernicus Global Land Services-based leaf area index (LAI), respectively (Boussetta & Balsamo, 2021). The overall effect of these modifications is to increase low vegetation cover, reduce high vegetation cover, and improve the representation of seasonal variations in leaf area index. To allow for better near-surface and atmospheric forecast skill, these changes were combined with additional land surface updates including a new soil moisture stress function, a new interpolation

 doi: 10.21957/crx2bn4is8

method to diagnose 2 m temperatures, and an improved representation of snow shadowing under high vegetation. Additional information about these changes to the land-surface model and their impact on 2 m temperature forecasts are provided by Ingleby et al. (2024).

Other updates to the IFS forecast model in Cycle 49r1 are summarised below:

- Improvements to short-wave radiation biases by assuming a liquid phase for mid-level convection if temperatures exceed –20ºC.
- Improvements to convection–surface coupling and downdraught scaling, which improves nighttime convective organisation.
- A revision of the diagnostic 10 m wind calculation, which removes a limiter and modifies the blending height, leading to reduced 10 m wind biases.
- Introduction of a time-varying source of stratospheric water vapour from methane oxidation.
- A new flexible treatment of aerosols in the IFS radiation code, which includes the potential for future 'hybrid' configurations that combine climatological and prognostic aerosol species.
- Many updates to the Copernicus Atmosphere Monitoring Service (CAMS) modelling systems (IFS-COMPO and IFS-GHG), including more up-to-date anthropogenic emissions, a new wetland emission model for methane, and major revisions to the aerosol model, including updated optical properties and a simple representation of stratospheric aerosols.

Data assimilation and observation usage

Cycle 49r1 includes substantial changes to the IFS data assimilation system, including several updates that improve near-surface weather forecasts. Daytime and nighttime 2 m temperature and 2 m humidity observations from SYNOP weather stations are now assimilated within the atmospheric 4D-Var system. Previous IFS versions assimilated only 2 m humidity during the daytime. This change has a strong positive impact on short-range 2 m temperature forecasts, particularly during the northern hemisphere winter. Several changes to the land data assimilation system also improve near-surface weather forecasts substantially. These include:

- a lapse-rate correction for 2 m temperature that accounts for differences between real-world and simulated orography
- updated background errors in the soil moisture analysis, and
- improved thinning of Interactive Multisensor Snow and Ice Mapping System (IMS) snow cover data combined with an updated diagnostic model for snow cover, which enables the activation of snow cover assimilation over mountainous areas.

These changes constitute a first step towards a more unified land data assimilation system, and they pave the way for further land–atmosphere coupled data assimilation developments (de Rosnay et al., 2022). Their impacts on 2 m temperature forecasts are described in more detail by Ingleby et al. (2024).

The Ensemble of Data Assimilations (EDA) receives a major upgrade in Cycle 49r1. Although the ensemble forecast resolution was increased from 18 km (TCo639) to 9 km (TCo1279) in Cycle 48r1, the resolution of the EDA was not changed. In Cycle 49r1 the horizontal grid spacing of the EDA outer loop resolution is reduced to ~9 km and the inner-loop grid spacing is reduced from ~100 km to ~40 km for the control member and to ~50 km for perturbed members. This substantial increase in horizontal resolution is made affordable by soft re-centring of each member (1 outer loop) around a more accurate control member (3 outer loops). Hólm et al. (2022) provide further background on the motivation for this soft re-centring approach. The combination of increased resolution and activation of SPP results in a general increase of EDA spread, though the magnitude of this effect varies regionally and with height. Figure 1 shows the changes in the spread of temperature, where the resolution increase and the soft re-centring contribute most above the boundary layer, and activation of SPP predominantly increases spread in the boundary layer. The combined effect is a 15–20% increase in spread in the extratropics, which leads to a significant improvement in the reliability of the EDA. These changes in spread impact the ensemble forecasts via initial perturbations but also deterministic analyses and forecasts, through the influence of the EDA on 4D-Var background error covariances. The impacts on ensemble variance as a function of horizontal scale are shown as power spectra in Figure 2. The increased EDA resolution in Cycle 49r1 removes the drop in ensemble variance previously evident at scales smaller than 200 km (wavenumber around 100). The variance spectrum at synoptic and planetary scales is also much smoother.

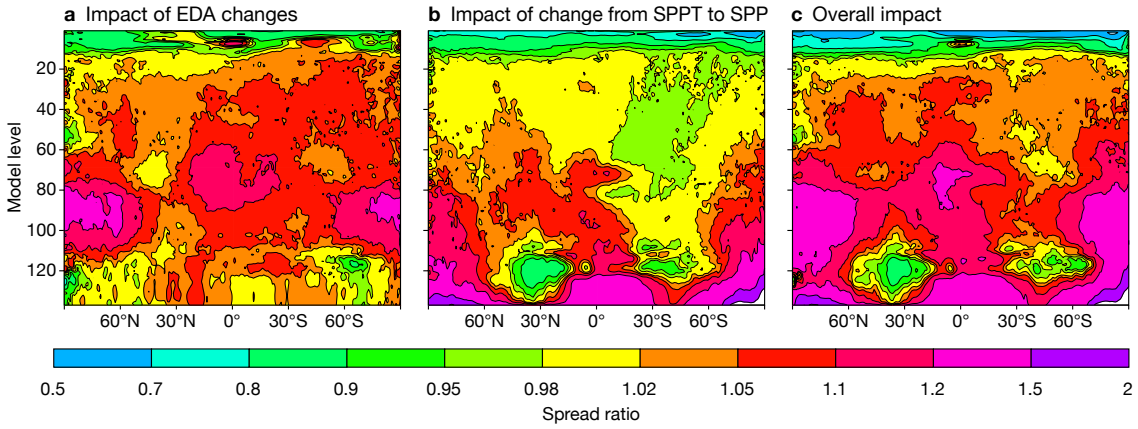

Figure 1 Contribution of EDA and model uncertainty changes to spread in Cycle 49r1 for zonal average temperature, showing (a) the impact of the soft re-centred EDA formulation, combined with a reduction of the horizontal grid-spacing of the EDA outer/inner-loop resolution from ~18 km/~100 km to ~9 km/~50 km – this is mostly above the boundary layer; (b) the impact of changing from SPPT to SPP at a grid spacing of ~9 km – this is mostly in the boundary layer; and (c) the total effect of soft re-centring, resolution change, and the switch to SPP. The plots are for the period of 17 December 2021 to 6 January 2022.

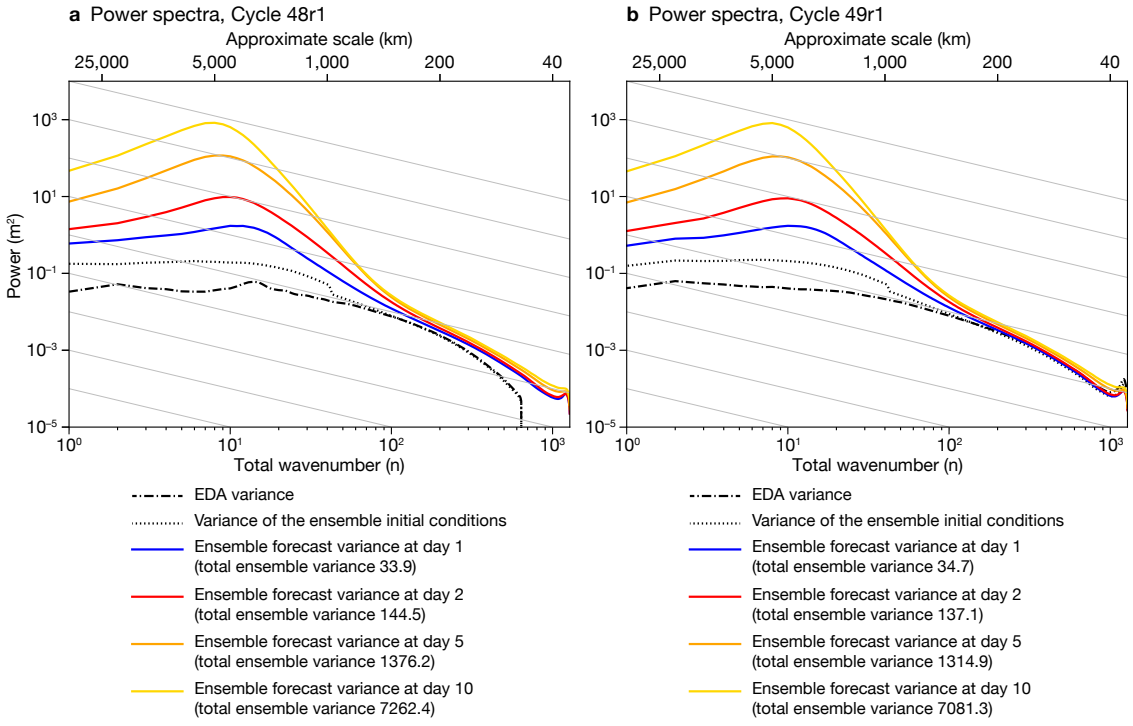

Figure 2 Global power spectra of the (ensemble) variance of the EDA and of the ENS for 250 hPa geopotential height against total wavenumber n, valid at 00 UTC during December 2023 – February 2024 for (a) Cycle 48r1 and (b) Cycle 49r1. The total ensemble variance (i.e. the sum over all wavenumbers) is provided in the legend. The use of a logarithmic x-axis means that wavenumbers become more tightly packed from left to right. To help discern the impact of this, diagonal lines represent contours of variance per linear unit length on the x-axis (with value proportional to the y-intercept). Approximate length scales are indicated on the top axis.

doi: 10.21957/crx2bn4is8

An important step towards a fully integrated Earth system assimilation system in Cycle 49r1 is the activation of microwave imaging radiances over sea-ice surfaces within the atmospheric 4D-Var component. This was not previously possible due to inadequate knowledge of either the sea-ice concentration (SIC) or the surface radiative properties of the sea ice. The problem has been solved using an innovative combination of machine learning and data assimilation to train a new sea-ice surface emissivity model for microwave radiances. A crucial aspect of the model is that it takes empirical input parameters that characterise the radiative properties of the sea ice. The empirical parameters summarise important aspects of the sea ice relating to things like the aging process of the ice as well as the snow cover on top. These aspects are poorly known, but they have a very strong control over the radiative signature of sea ice observed by microwave imagers. Using an observation space control variable (often referred to as a sink variable), the 4D-Var control vector is extended to estimate SIC and the empirical sea-ice properties at each observation location. The addition of data from Advanced Microwave Scanning Radiometer 2 (AMSR2) and Global Precipitation Measurement Microwave Imager (GMI) in sea ice and neighbouring areas improves forecast scores in the vicinity of Antarctica by around 0.5% out to day 4. The SIC retrievals are of good quality and could be provided as an input to the ocean/sea-ice data assimilation system in a future IFS cycle. An example of the quality of the SIC observations is given in Figure 3, which shows the evolution of a giant iceberg (note that microwave imagers sense any ice coverage on the ocean surface, which differs from stricter definitions of sea ice). Further details can be found in Geer (2023, 2024).

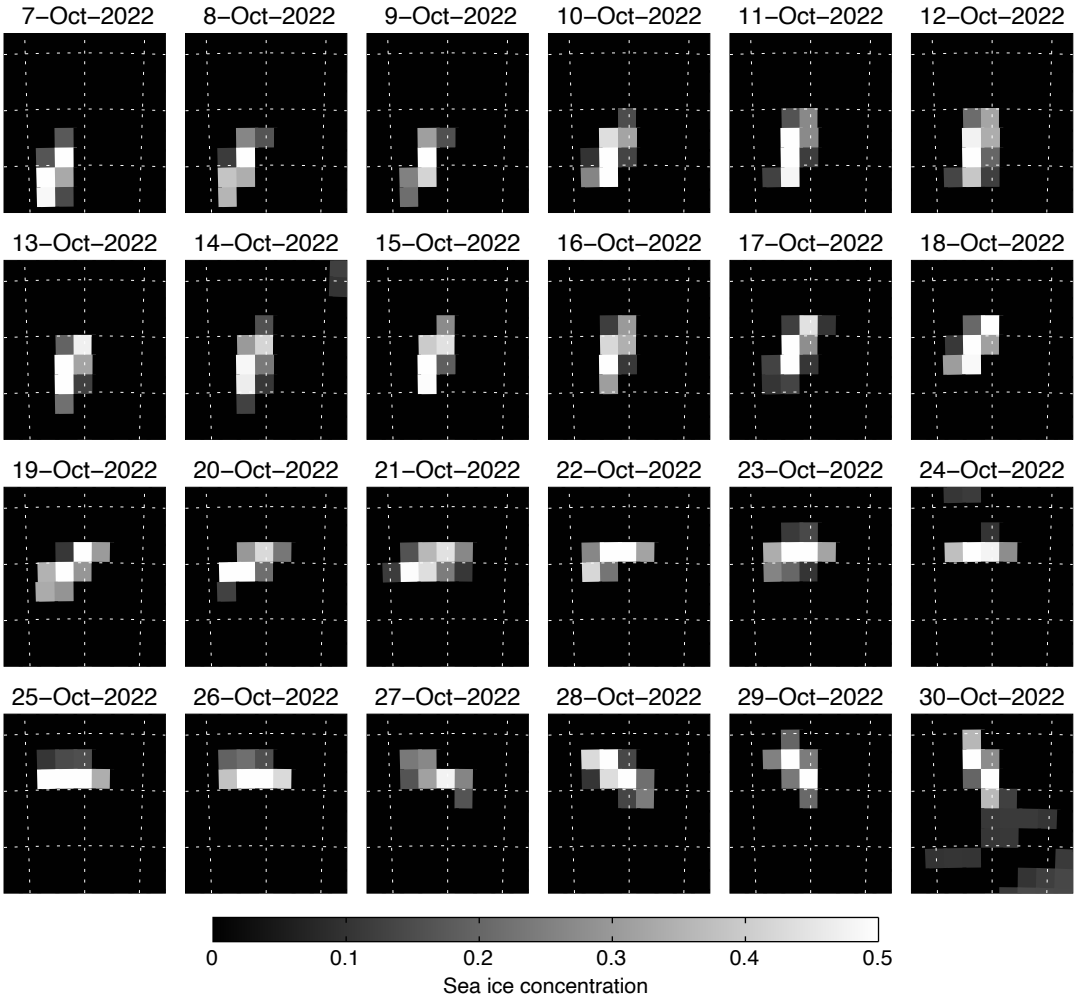

Figure 3 Daily maps of the extent of long-lived giant iceberg A76A during October 2022, based on the new AMSR2 SIC retrievals within atmospheric 4D-Var. Iceberg A76A was at this time around 135 km by 26 km in size and rotating in the currents of the Southern Ocean near the Antarctic Peninsula. The pixel size of the AMSR2 retrievals is 40 km by 40 km. Grid lines are shown every 1° latitude and 2° longitude, and the projection is centred on 59.25°S, 50°W. The figure is re-used under creative commons attribution licence from Geer (2024, *https://doi.org/10.1002/qj.4797*).

Other data assimilation and observation usage contributions to Cycle 49r1 include the following:

- A 140% increase in the use of satellite microwave humidity data.
- Activation of additional channels from the Advanced Microwave Sounding Unit-A and the Special Sensor Microwave Imager/Sounder.
- Several updates to non-microwave observations, including reduced thinning of Spinning Enhanced Visible and InfraRed Imager data, assimilation of ground-based Global Navigation Satellite System data, and scene-dependent observation errors for Cross-track Infrared Sounders.
- A vertical extension of Global Navigation Satellite System Radio Occultation assimilation from 50 km to 60 km altitude.
- An upgrade to version 13.2 of the Radiative Transfer for TOVS (RTTOV) model and other updates in the radiance observation operator.
- Activation of Variational Quality Control (VarQC) in the first 4D-Var minimisation.
- Activation of balance constraints above 20 km, which allows stratospheric sounding instruments to generate geostrophically balanced increments from the start of the assimilation window.

Impact on medium-range and sub-seasonal forecasts

Cycle 49r1 substantially improves short- and medium-range forecasts of 2 m temperature and 10 m wind speeds. The largest impacts on 2 m temperature forecasts are for the winter months in the northern hemisphere (Figure 4), where the Continuous Ranked Probability Score (CRPS) is improved by 11% at day 1 and 2% at day 10. In short-range forecasts, the biggest improvements are over Asia and Canada (Figure 5). These improvements reflect the combined impact of many contributions, including the assimilation of 2 m temperature observation data, upgrades to 4D-Var and land-surface data assimilation methodology, and improvements to the IFS land surface model (Ingleby et al., 2024).

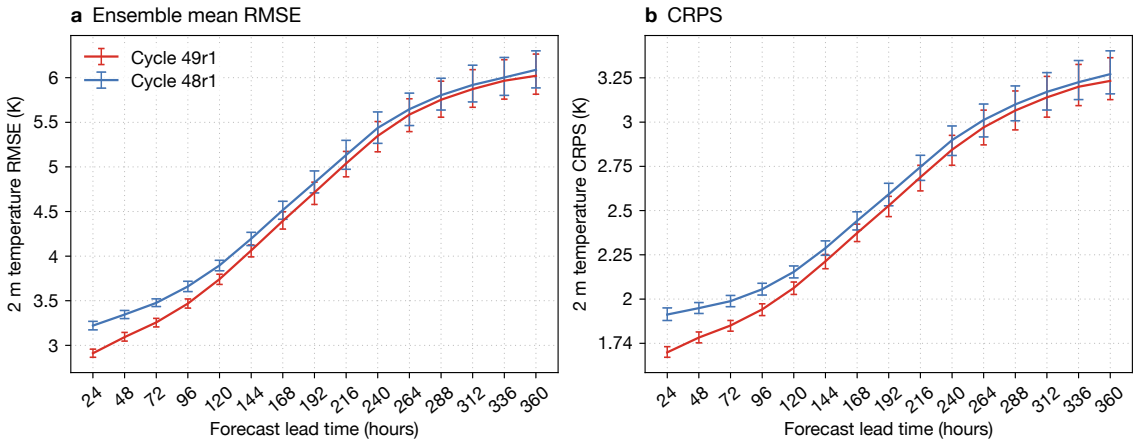

Figure 4 The charts show (a) the root-mean-square error (RMSE) of the ensemble mean and (b) the continuous ranked probability score (CRPS) for 2 m temperature from Cycle 48r1 (blue) and Cycle 49r1 (red), verified against observations and averaged over the northern hemisphere. All scores are calculated using 50 perturbed members from 75 forecasts initialised daily between 1 December 2022 and 13 February 2023.

doi: 10.21957/crx2bn4is8

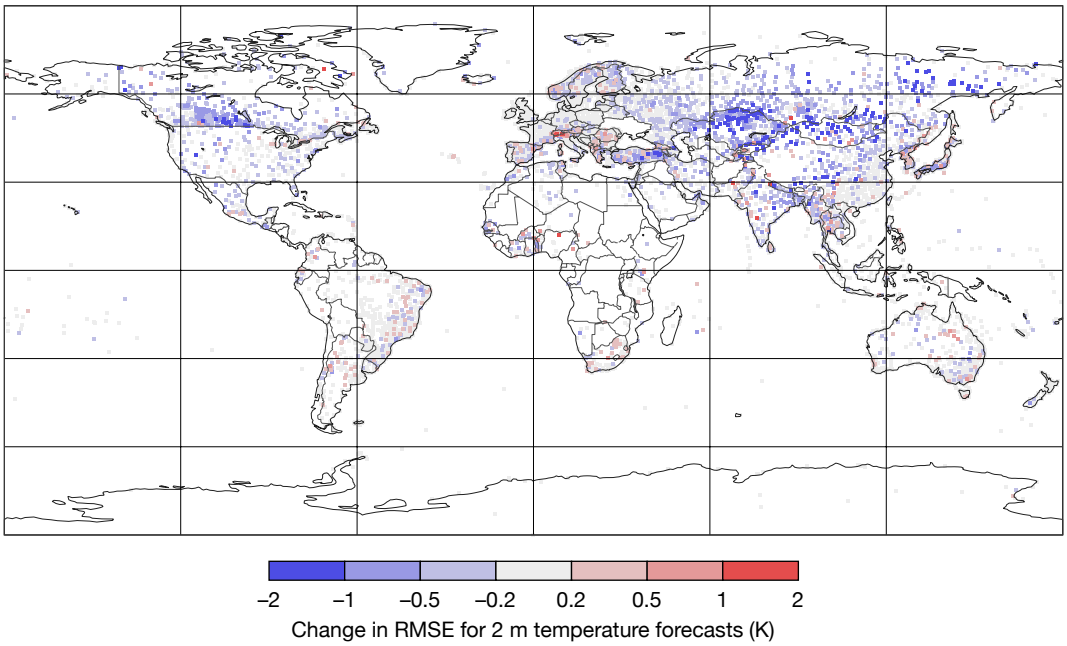

Figure 5 Change in root-mean-square error (RMSE) for 24-hour deterministic forecasts of 2 m temperature at 00 and 12 UTC between December 2022 and February 2023 inclusive. Blue colours indicate improvements in IFS Cycle 49r1 with respect to IFS Cycle 48r1.

Forecasts of 10 m wind speed are improved throughout the year. The largest impacts are for the winter months of the northern hemisphere (Figure 6), where the CRPS is improved by 12% at day 1 and 6% at day 10. The major contributors to improved ensemble forecasts of 10 m wind speed are the increased spread in the boundary layer associated with the switch to the SPP scheme for model uncertainty; improvements to the diagnostic 10 m wind calculation; and the combination of updates to the land-surface model.

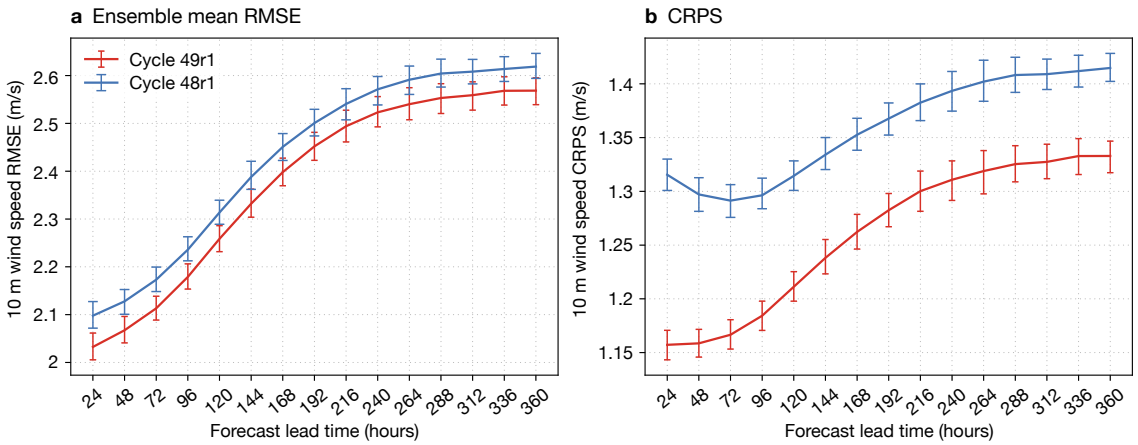

Figure 6 As Figure 4, but for 10 m wind speeds.

Figures 7 and 8 summarise the impact of Cycle 49r1 relative to Cycle 48r1. They use several metrics of deterministic and probabilistic forecast skill for a range of variables and levels across medium-range lead times. Cycle 49r1 has an overall positive impact on both deterministic and ensemble forecast skill scores. For example, CRPS and anomaly correlations are both improved in 73% of comparisons shown in Figure 8. The impact in the tropics is more mixed, especially for verification against analyses. Some of the negative impacts are a consequence of interactions between the new EDA configuration and other contributions to Cycle 49r1. In particular, the increased EDA resolution and the introduction of SPP both have a non-uniform impact on the EDA forecast spread (see Figure 1). This spread informs background errors of the 4D-Var system and provides perturbations for the initialisation of the ensemble forecasts. The final configuration of Cycle 49r1 reflects a compromise that balances evidence from observation-based verification, analysis-based verification, and observation–background/observation–analysis statistics. This involved a tuning process that uniformly reduced the background errors provided to the 4D-Var system by 16% and separately a 15% reduction of the amplitude of the singular vector perturbations added to ensemble initial conditions.

 doi: 10.21957/crx2bn4is8

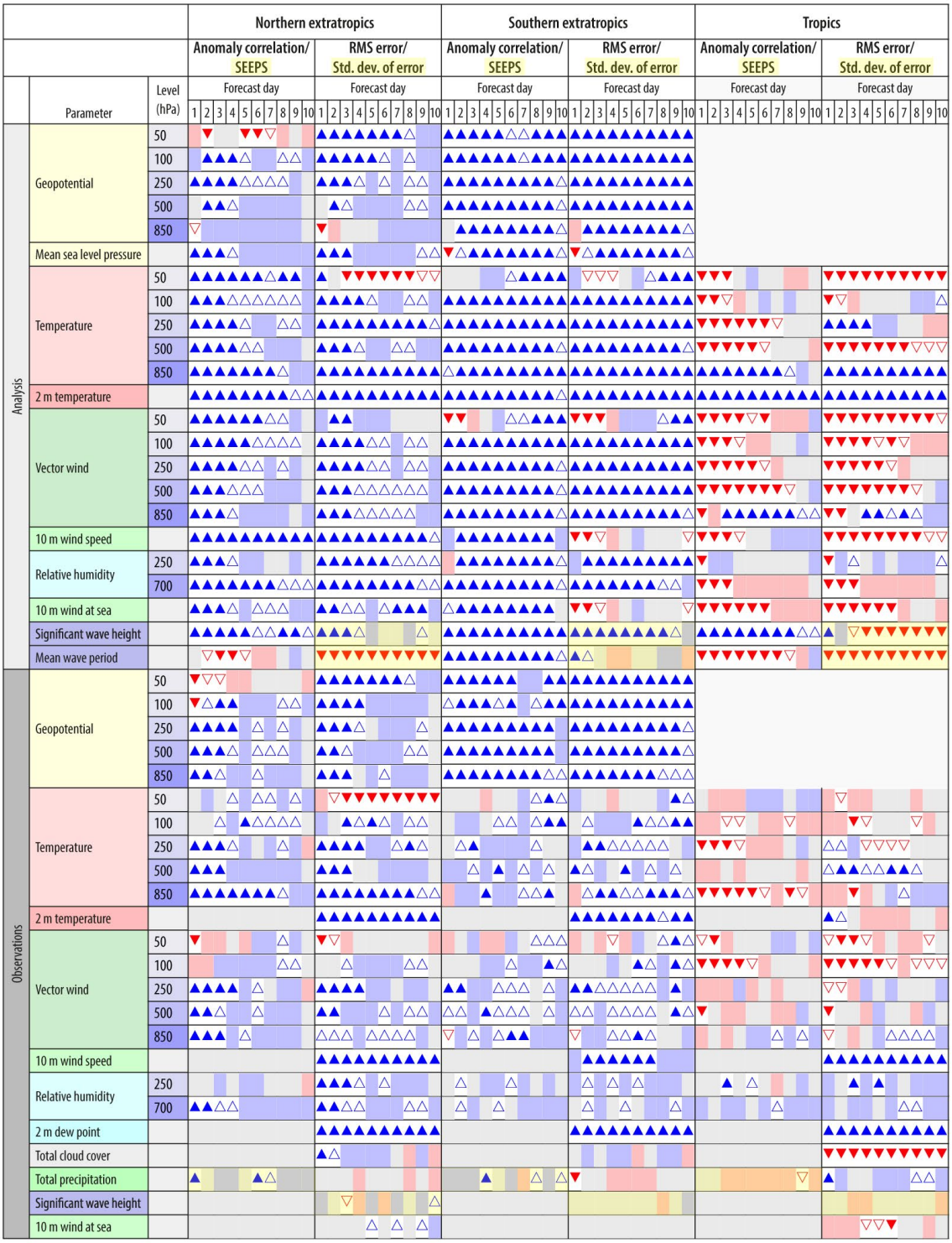

Symbol legend: for a given forecast step...

- ▲ 49r1 better than 48r1 statistically significant with 99.7% confidence
- △ 49r1 better than 48r1 statistically significant with 95% confidence
- 49r1 better than 48r1 statistically significant with 68% confidence
- no significant difference between 48r1 and 49r1
- 49r1 worse than 48r1 statistically significant with 68% confidence
- ▽ 49r1 worse than 48r1 statistically significant with 95% confidence
- ▼ 49r1 worse than 48r1 statistically significant with 99.7% confidence

Figure 7 Summary scorecard comparing the difference between control forecasts from IFS Cycle 49r1 and IFS Cycle 48r1 using anomaly correlation coefficients and the root-mean-square error (RMSE). Note that total precipitation is evaluated using the Stable Equitable Error in Probability Space (SEEPS) score rather than correlation, and wave parameters are evaluated using the standard deviation of errors rather than RMSE. Blue colours indicate improvements in IFS Cycle 49r1 with respect to IFS Cycle 48r1. Scores are calculated from more than 1,000 forecasts initialised at 00 and 12 UTC between 1 June 2022 and 8 August 2024.

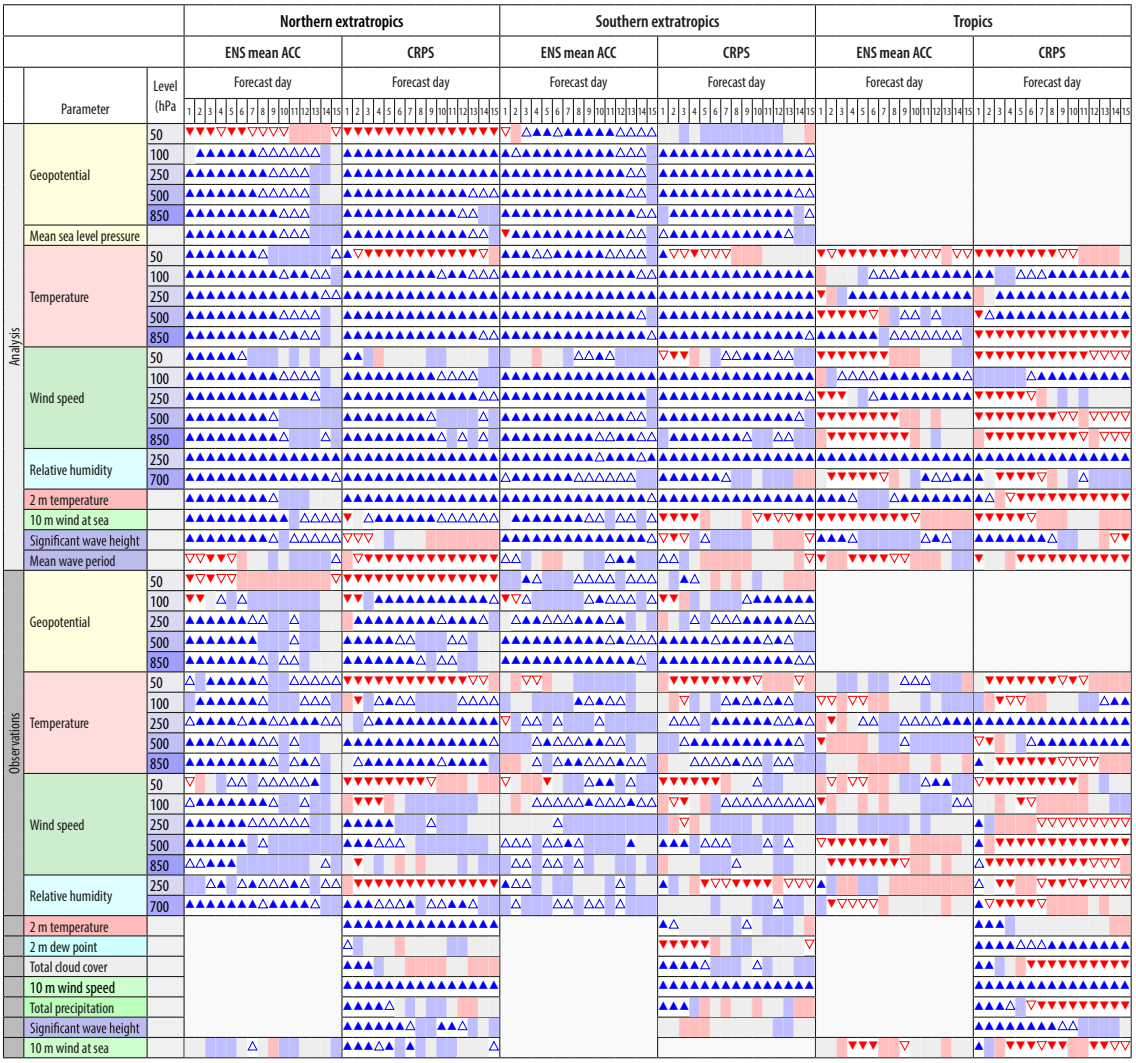

Symbol legend: for a given forecast step...

- ▲ 49r1 better than 48r1 statistically significant with 99.7% confidence
- △ 49r1 better than 48r1 statistically significant with 95% confidence
- 49r1 better than 48r1 statistically significant with 68% confidence
- no significant difference between 48r1 and 49r1
- 49r1 worse than 48r1 statistically significant with 68% confidence
- ▽ 49r1 worse than 48r1 statistically significant with 95% confidence
- ▼ 49r1 worse than 48r1 statistically significant with 99.7% confidence

Figure 8 Summary scorecard comparing the difference between ensemble forecasts with IFS Cycle 49r1 and IFS Cycle 48r1, using the anomaly correlation coefficient (ACC) of the ensemble mean and the continuous ranked probability score (CRPS). Blue colours indicate improvements in IFS Cycle 49r1 with respect to IFS Cycle 48r1. Scores are calculated using 50 perturbed ensemble members from more than 400 forecasts initialised at 00 UTC between 1 June 2022 and 8 August 2024.

Despite significant changes to the EDA and model uncertainty representations, the scale-dependent growth of forecast uncertainty is, to first order, very similar in Cycle 49r1 and Cycle 48r1 (Figure 2). Nevertheless, there is a systematic reduction in synoptic-scale ensemble variance at medium-range lead times that provides a 10% improvement to the over-dispersion in the storm tracks in Cycle 48r1. This improves both ensemble reliability and sharpness (not shown).

Tropical cyclone (TC) intensity and position errors are generally similar in Cycle 49r1 and Cycle 48r1 (Figure 9). The most important change is the significant increase in the ensemble spread of TC intensity, especially at earlier lead times, which is mainly a consequence of the new EDA configuration. This change improves the reliability of TC intensity forecasts, as seen in ensemble spread and ensemble mean root-mean-square error (RMSE) moving closer to each other. In addition, the switch from SPPT to SPP results in a systematic increase in the frequency of tropical cyclones. This increase is likely to be detrimental for weaker systems, which were already overestimated compared to observations, but beneficial for deeper systems, which remain underestimated in Cycle 49r1.

doi: 10.21957/crx2bn4is8

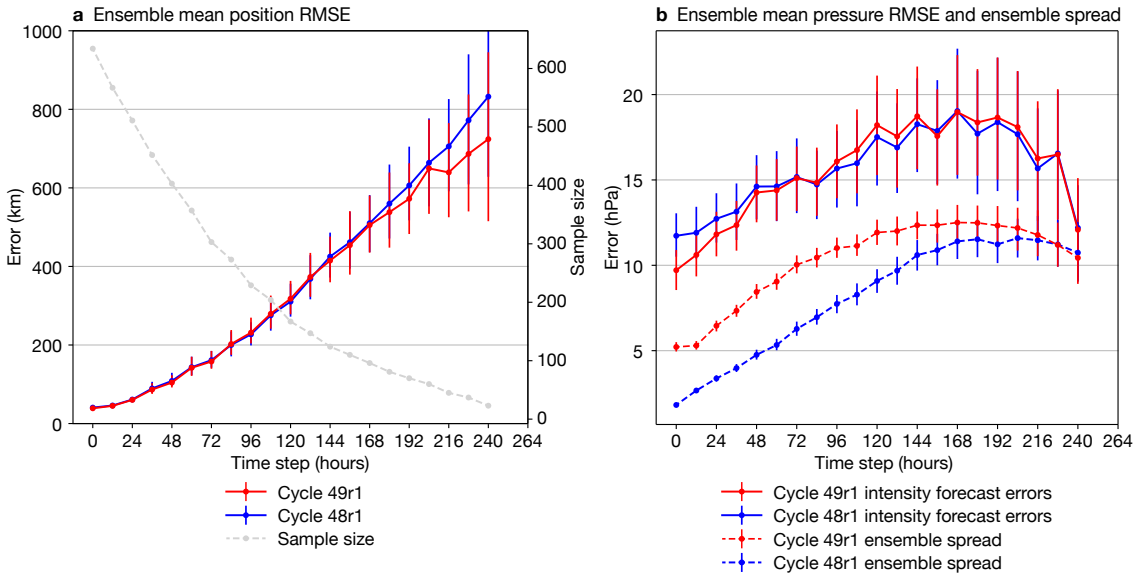

Figure 9 Tropical cyclone position and intensity forecast errors in IFS Cycle 49r1 compared to IFS Cycle 48r1, showing (a) ensemble mean position forecast errors of Cycle 49r1 and Cycle 48r1 and (b) intensity (central pressure) forecast errors (solid lines) and ensemble spread (dashed lines) of Cycle 49r1 and Cycle 48r1. The vertical error bars represent 95% confidence intervals. Tropical cyclone scores are calculated using 50 perturbed members from forecasts initialised daily between 3 June 2022 and 29 March 2024.

An undesirable feature of TC forecasts in Cycle 49r1 is the increased frequency of unrealistic TC structures that are not axisymmetric and associated very strong winds at initialisation time in perturbed ensemble members. These artefacts are a property of the ensemble initial conditions rather than the forecast model and dissipate within the first 12 hours of the forecast without significantly changing medium-range TC forecast quality. This issue is a consequence of the way ensemble initial conditions are derived from perturbations taken from a more realistic EDA and then re-centred around a reference analysis. It was previously described by Lang et al. (2015) and will be addressed with a revision of the ensemble initial perturbations methodology in a forthcoming IFS upgrade.

The ECMWF sub-seasonal forecasting system, which provides an overview of potential weather conditions up to 46 days ahead, is also updated in Cycle 49r1. The most robust impacts on weekly mean forecast anomalies are small but statistically robust changes in ensemble spread, which are driven by the switch from SPPT to SPP. These changes are most evident in the tropics, where ensemble spread in the free atmosphere is reduced by several per cent, which represents a slight improvement in ensemble reliability relative to Cycle 48r1. Despite these changes to ensemble spread, deterministic and probabilistic weekly mean anomaly scores are generally very similar in Cycle 49r1 and Cycle 48r1.

Despite the limited impact on weekly mean scores aggregated over large regions, Cycle 49r1 improves the bivariate correlation skill of Madden–Julian Oscillation (MJO) forecasts at lead times greater than 15 days. These changes are associated with improved MJO reliability at sub-seasonal lead times, which is a consequence of the switch from SPPT to SPP.

System configuration changes and updated products

Cycle 49r1 introduces new and revised diagnostic products, including a harmonisation of convection-related parameters. All relevant applications and products in Cycle 49r1 use consistent definitions of Most Unstable Convective Available Potential Energy (MUCAPE) and Most Unstable Convective Inhibition (MUCIN). The original parameters for Convective Available Potential Energy (CAPE) and Convective Inhibition (CIN) are discontinued. Other product changes include new graphical products for true-colour simulated satellite imagery, new parameters related to heat stress (Wet Bulb Globe Temperature, Heat Index, Humidex, Wind Chill Temperature, Universal Thermal Climate Index), and an extension of probabilistic clear-air turbulence products to include contributions from non-orographic gravity-wave dissipation outside of convection areas.

Cycle 49r1 also introduces several major changes to the configuration of operational systems:

- The wave model is now run with the same native grid as the atmospheric model in all forecast systems, and the number of frequencies in wave spectra output is reduced from 36 to 29. For example, for medium-range ensemble forecasts (ENS), the native grid of the wave model will change from a 14 km reduced latitude–longitude grid to use the same TCo1279 (~9 km) grid as the atmosphere.
- Cycle 48r1 increased the horizontal resolution of ENS from TCo639 to TCo1279. One consequence of this upgrade was to make the unperturbed ENS control forecast scientifically equivalent (though not computationally identical) to the high-resolution deterministic forecast (HRES). Although nearly identical, HRES and the ENS control forecast retained some differences in lead time (10 days vs 15 days), output frequencies, and dissemination times. In Cycle 49r1, HRES and the ENS control forecast become scientifically and computationally identical and both are run for 15 days at 00 UTC and 12 UTC. The superfluous ENS control forecast will be stopped in a future IFS upgrade, and the data stream currently known as HRES will become known as the 'control' forecast. The retitled control forecast will be available on the same schedule as the current HRES (i.e. earlier than the perturbed ENS forecast members).
- Cycle 49r1 introduces new configurations for medium-range and sub-seasonal retrospective ensemble forecasts (also known as 're-forecasts' or 'hindcasts'). The ensemble size of re-forecasts (ten perturbed members and one control member) is unchanged from Cycle 48r1. However, the frequency of re-forecasts is changed for both systems. In Cycle 48r1, both medium-range and sub-seasonal re-forecasts were run every Monday and Thursday for the previous 20 years. In Cycle 49r1, sub-seasonal re-forecasts are run every odd day of the month over the previous 20 years (i.e. 1st, 3rd, 5th…, excluding 29th February) and medium-range re-forecasts are run every other odd day of the month over the previous 20 years (i.e. 1st, 5th, 9th…, excluding 29th February). There are several advantages to these new re-forecast configurations: (i) The increased frequency of sub-seasonal re-forecasts benefits skill assessment and the calibration of real-time forecasts. (ii) The use of fixed re-forecast dates enables direct comparisons with seasonal re-forecasts and between sub-seasonal re-forecasts produced in different years. (iii) The common dates for medium-range and sub-seasonal re-forecasts facilitate resolution sensitivity studies and provide opportunities for the generation of calibrated dual-resolution ensemble products.

Summary and outlook

IFS Cycle 49r1 brings substantial changes to data assimilation methodology, the use of observations, and the underlying IFS forecast model. These changes have an overall positive impact on both deterministic and ensemble forecasts and significantly improve 2 m temperature and 10 m wind forecasts, particularly for the winter months in the northern hemisphere. The improvements in near-surface weather conditions reflect the combined impact of many contributions, but especially the assimilation of 2 m temperature observation data; upgrades to 4D-Var and land-surface data assimilation methodology; improvements to the IFS land surface model; the switch to the SPP scheme for model uncertainty; and improvements to the diagnostic 10 m wind calculation. The assimilation of microwave imaging radiances over sea-ice surfaces is an important step towards Earth system data assimilation, in which the different components are integrated in a coupled data assimilation framework (de Rosnay et al., 2022). Other major contributions to Cycle 49r1 include the increased resolution and soft re-centring of the EDA; the increased usage of satellite observations; the increased resolution of the ocean wave model; and changes to the frequency of medium-range and sub-seasonal re-forecasts. Looking ahead, the next update of the IFS (Cycle 49r2) will build upon Cycle 49r1 and serve as the foundation for the next ECMWF reanalysis (ERA6) and seasonal forecast system (SEAS6). Cycle 49r2 will not be implemented operationally for medium-range or sub-seasonal forecasts, but all developments for ERA6 and SEAS6 will be included as part of the next operational IFS upgrade (Cycle 50r1).

 doi: 10.21957/crx2bn4is8

Further reading

Bidlot, **J.-R**. & **P. Janssen**, 2024: Ocean-wave-related changes in the next model upgrade, *ECMWF Newsletter* **No. 179**, 18–25. *https://doi.org/10.21957/jb9py41a6f*

Boussetta, **S.** & **G. Balsamo**, 2021: CONFESS Vegetation dataset of Land Use/Land Cover and Leaf Area Index. CONFESS D1.1. *https://confess-h2020.eu/wp-content/uploads/2021/08/confess-d1-1-v1-0-.pdf*

de Rosnay, **P.**, **P. Browne**, **E. de Boisséson**, **D. Fairbairn**, **Y. Hirahara**, **K. Ochi et al.**, 2022: Coupled data assimilation at ECMWF: current status, challenges and future developments. *QJRMS*, **148**(747), 2672–2702. *https://doi.org/10.1002/qj.4330*

Geer, **A.J.**, 2023: Combining machine learning and data assimilation to estimate sea ice concentration, *ECMWF Newsletter* **No. 177**, 14–21. *https://doi.org/10.21957/agh93vs26*

Geer, **A.J.**, 2024: Joint estimation of sea ice and atmospheric state from microwave imagers in operational weather forecasting. *QJRMS*. *https://doi.org/10.1002/qj.4797*

Hólm, **E.**, M. Bonavita, & S. Lang, 2022: Soft re-centring Ensemble of Data Assimilations. *ECMWF Newsletter* **No. 171**. *https://www.ecmwf.int/en/newsletter/171/news/soft-re-centring-ensemble-data-assimilations*

Ingleby, **B.**, **G. Arduini**, **G. Balsamo**, **S. Boussetta**, K. Ochi, E. Pinnington et al., 2024: Improved two-metre temperature forecasts in the 2024 upgrade. *ECMWF Newsletter* **No. 178**, 24–29. *https://doi.org/10.21957/bi49s20qa8*

Lang, **S.T.**, **M. Bonavita** & **M. Leutbecher**, 2015: On the impact of re-centring initial conditions for ensemble forecasts. *QJRMS*, **141**(692), 2571–2581. *https://doi.org/10.1002/qj.2543*

McNorton, **J.** & **G. Balsamo**, 2023: An urban scheme for the IFS, *ECMWF Newsletter* **No. 175**, 18–19. *https://www.ecmwf.int/en/newsletter/175/news/urban-scheme-ifs*

doi: 10.21957/crx2bn4is8